A Review of Parameterizations for Enthalpy and Momentum Fluxes from Sea Spray in Tropical Cyclones

SYDNEY SROKA[a] AND KERRY EMANUEL[a]

[a] *Massachusetts Institute of Technology, Cambridge, Massachusetts*

(Manuscript received 29 January 2021, in final form 21 May 2021)

ABSTRACT: The intensity of tropical cyclones is sensitive to the air–sea fluxes of enthalpy and momentum. Sea spray plays a critical role in mediating enthalpy and momentum fluxes over the ocean's surface at high wind speeds, and parameterizing the influence of sea spray is a crucial component of any air–sea interaction scheme used for the high wind regime where sea spray is ubiquitous. Many studies have proposed parameterizations of air–sea flux that incorporate the microphysics of sea spray evaporation and the mechanics of sea spray stress. Unfortunately, there is not yet a consensus on which parameterization best represents air–sea exchange in tropical cyclones, and the different proposed parameterizations can yield substantially different tropical cyclone intensities. This paper seeks to review the developments in parameterizations of the sea spray–mediated enthalpy and momentum fluxes for the high wind speed regime and to synthesize key findings that are common across many investigations.

KEYWORDS: Parameterization; Tropical cyclones; Air-sea interaction

1. Introduction

Parameterizations of air–sea exchange represent a large source of uncertainty in tropical cyclone (TC) intensity forecasts (Emanuel 1995; Black et al. 2007; Powell et al. 2003; Donelan et al. 2004; Green and Zhang 2013, 2014; Torn 2016; Ma et al. 2017; Richter et al. 2016; Chen et al. 2018; Nystrom and Zhang 2019; Nystrom et al. 2020). Improving the representation of air–sea enthalpy and momentum fluxes in particular is key to improving intensity forecast accuracy. Since sea spray has been shown to mediate a significant percentage of the total enthalpy and momentum fluxes in TCs (Andreas and Emanuel 2001, hereafter AE1; Andreas 2004; Zhao et al. 2006; Andreas 2010; Richter and Stern 2014; Mueller and Veron 2014b; Troitskaya et al. 2018b; Peng and Richter 2017, 2019, 2020), bulk parameterizations have begun to incorporate the microphysics associated with sea spray–mediated fluxes. In particular, many of the investigations specifically focus on the way sea spray affects the bulk surface exchange coefficients for enthalpy C_K and momentum C_D.

The bulk flux formulation for the air–sea enthalpy flux H_K is typically of the form

$$H_K = \rho_a C_K |U|(k^* - k), \tag{1}$$

where ρ_a is the density of air, $|U|$ is the magnitude of the wind speed at a reference height, k^* is the saturation specific enthalpy at the surface, and k is the specific enthalpy at a reference height. The typical reference height is 10 m and is indicated with a subscript (e.g., U_{10}). The specific enthalpy is $k = L_v q + c_p T$, where L_v is the latent heat of vaporization, q is the specific humidity, c_p is the specific heat of air, and T is the temperature.

The bulk flux formulation for the unidirectional air–sea momentum flux (or surface stress) τ is typically of the form

$$\tau = \rho_a C_D |U| U. \tag{2}$$

The momentum flux (or sea surface drag) coefficient C_D is used to relate the friction velocity u_* to the velocity at the reference height such that $C_D = u_*^2/U_{10}^2$. Many of the experiments described in this review which measure wind speed profiles in order to calculate C_D assume that the air near the surface is neutrally stable, and thus the wind profile is

$$U(z) = \frac{u_*}{\kappa} \ln\left(\frac{z}{z_0}\right), \tag{3}$$

where κ is the von Kármán constant (=0.4) and z_0 is the roughness length (Monin and Obukhov 1954).

Frameworks that simulate TCs and forecast TC intensity are sensitive to the details of the surface exchange coefficient formulations because several key quantities are functions of the coefficients or their ratio C_K/C_D. For example, the maximum azimuthal wind speed is proportional to $(C_K/C_D)^{1/2}$, and both the central pressure deficit and the ratio of the outer scale to the radius of maximum wind depend on the ratio C_K/C_D (Emanuel 1986, 1995).

Figures 1 and 2 show some of the proposed exchange coefficients for enthalpy flux and momentum flux, respectively. The ratio of these coefficients is shown in Fig. 3 when possible. The data shown in Fig. 2 from Powell et al. (2003) correspond to the 10–150 m surface layer depth estimate and measurements, and the data from French et al. (2007) correspond to the average C_D from measurements in the 2.5 m s^{-1} bin around each data point. The error bars from Powell et al. (2003), French et al. (2007), and Richter and Stern (2014) indicate the 95% confidence interval,

Denotes content that is immediately available upon publication as open access.

Sroka's ORCID: 0000-0002-8225-7568.

Corresponding author: Sydney Sroka, ssroka@mit.edu

DOI: 10.1175/JPO-D-21-0023.1

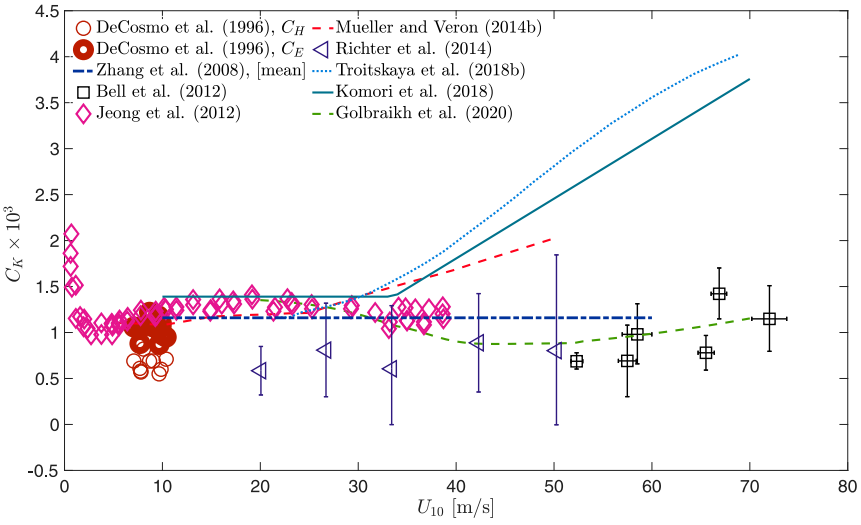

FIG. 1. The sea surface enthalpy exchange coefficient C_K as a function of U_{10} from many of the studies considered throughout this review. Note that DeCosmo et al. (1996) estimated the sensible heat transfer coefficient C_H and the latent heat transfer coefficient C_E separately.

the error bars from Holthuijsen et al. (2012) represent the 90% confidence interval, and the error bars from Bell et al. (2012) represent one standard deviation away from the mean. The coefficients from Mueller and Veron (2014b) correspond to the case with the sea spray generation function from Mueller and Veron (2009a). Zhang et al. (2008) reported that the mean and standard error of C_K from their measurements was $(1.16 \pm 0.07) \times 10^{-3}$; for clarity, only the mean is shown in Fig. 1. The coefficients from Troitskaya et al. (2018b) correspond to field conditions and a wave age of 3.5 as defined therein. Experimental results are shown with open symbols while theoretical profiles that are informed by experiments are shown with lines. The experimental data were collected from published figures using digitizing software, which introduces an error that should be at most 5%. The wide range of values and large error bars in these figures are a reflection of how challenging it is to determine how the exchange coefficients scale with the 10-m wind speed. Numerical models that use constant valued exchange coefficients often set both coefficients equal to 1.0×10^{-3} such that their ratio is unity.

Several reviews of sea spray production and its effects on air–sea exchange have appeared, beginning with Bortkovskii (1987) and continuing with Bryant and Akbar (2016) and

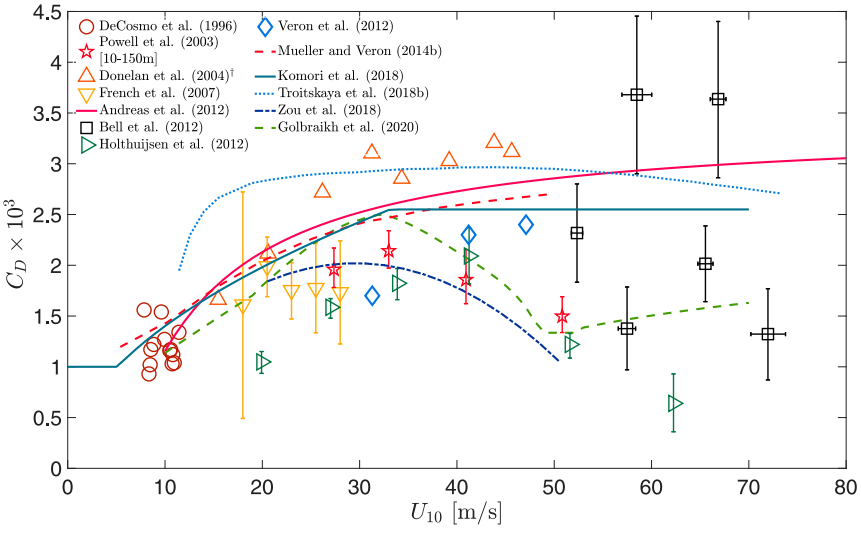

FIG. 2. The sea surface drag coefficient C_D as a function of U_{10} from many of the studies described throughout this review. Most studies find that C_D increases with U_{10} until about $U_{10} = 30\,\mathrm{m\,s^{-1}}$. The plotted Donelan et al. (2004) data reflects the corrections published in Curcic and Haus (2020) for the momentum budget method.

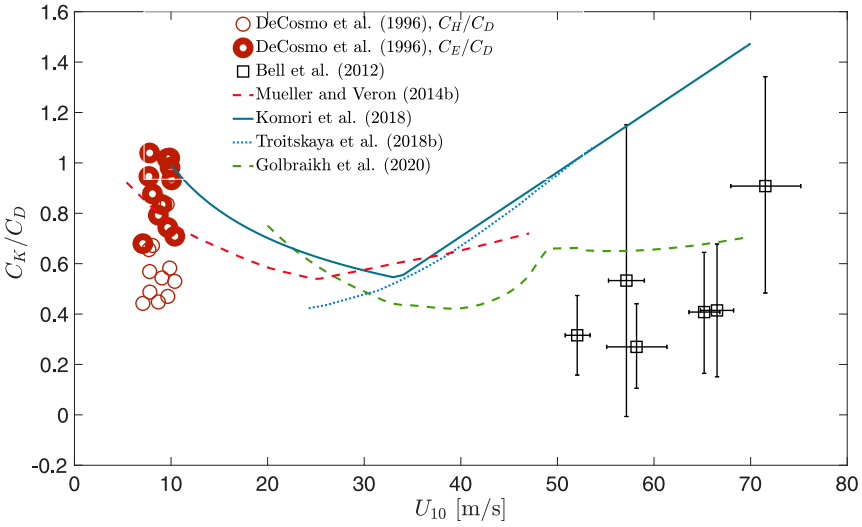

FIG. 3. The ratio of the sea surface enthalpy exchange coefficient to the sea surface drag coefficient from many of the studies described throughout this review that estimated both.

Veron (2015). This review updates the earlier reviews and focuses on parameterizations of enthalpy and momentum fluxes in the high wind speed regime that account for sea spray–mediated exchange, with the goal of assisting the modeling community since there have been many parameterizations proposed and TC intensity is sensitive to the details of the surface exchange algorithms. Section 2 reviews the theoretical work that confirmed surface exchange coefficients, and therefore surface processes, were important for accurate TC intensity estimates. Sections 3 and 4 review the results from field campaigns and laboratory experiments, respectively, that directly or indirectly measured air–sea fluxes at extreme wind speeds in the presence of spray. Section 5 reviews the contributions from Edgar Andreas, with a focus on how his microphysical model was used to estimate the enthalpy and momentum fluxes from sea spray under extreme wind speeds. Section 6 reviews numerical experiments of evaporating sea spray, particularly those from Lagrangian particle experiments. Finally, section 7 summarizes a few of the key developments in sea spray generation functions for the high wind speed regime.

2. Theoretical models

a. *Early evidence of the importance of C_K and C_D for tropical cyclones*

The air–sea fluxes of enthalpy and momentum have long been acknowledged as important components of TC dynamics (Byers 1944; Kleinschmidt 1951; Riehl 1950, 1954; Palmén and Riehl 1957; Malkus and Riehl 1960). Early work on the impact of the air–sea enthalpy flux on a TC includes Riehl (1950), who showed how the enthalpy flux from the ocean was critical for maintaining the pressure gradient in the core of a TC. Riehl (1954) remarked that sea spray is clearly an important mediator of air–sea flux since spray dramatically increases the surface area available for sensible and latent heat exchange near the high-speed, low-pressure region of the TC. Palmén and Riehl (1957) related the heat flux from the ocean to both the central pressure deficit and the mean tropospheric temperature, and also studied the air–sea flux of momentum through a budget analysis. Malkus and Riehl (1960) estimated the sensible and latent heat flux from the ocean as a function of radius from the storm's center and used a dynamic model of a steady state, mature storm to study the momentum flux.

Some of the first studies that investigated the role of surface fluxes from the ocean in TC maintenance also estimated values of the exchange coefficients. Palmén and Riehl (1957) estimated the drag coefficient at various radial distances from mean wind measurements; they found that it generally decreased away from the storm's center and ranged from 1.4×10^{-4} to 2.1×10^{-3}. They also found that the inflow layer depth was deeper closer to the center of the storm. Malkus and Riehl (1960) used an empirical drag coefficient that ranged from 1.1×10^{-3} to 3.0×10^{-3} and estimated the sensible and latent heat exchange coefficients by using the results from their dynamical model to solve the bulk exchange equations for the coefficients. They found that the sensible heat exchange coefficient decreased closer to the storm's center where the wind speeds are higher, while the latent heat exchange coefficient slightly increased closer to the storm's center.

Several early studies that estimated the exchange coefficients from observations or simulations of TCs emphasized the challenges involved. Miller (1962) made some of the first estimates of these coefficients from observations using both flight level and ship data from Hurricane Helene (1958). After assuming a steady state, axially symmetric cyclone, Miller (1962) solved for the coefficients using measurements of the radial transport of angular momentum and moist static energy. His calculations showed that the enthalpy exchange coefficient and drag coefficient were largest at the center of the storm, 3.6×10^{-3} and 3.2×10^{-3}, respectively, and decreased to 3.2×10^{-3} and 2.4×10^{-3}, respectively, at 60 n mi (1 n mi = 1.852 km) radially away from the storm's center. However, Miller repeatedly

stressed the limitations of this dataset, particularly how a lack of reliable radial wind measurements required estimating the radial winds indirectly, and urged the community to invest in a campaign to gather more measurements to more accurately determine the exchange coefficients. Hawkins and Rubsam (1968) also used aircraft measurements to estimate the drag coefficient. They calculated surface stress by assuming that it balanced radial advection of absolute angular momentum and found that C_D increased with U_{10} for wind speeds up to about 46 m s^{-1}. However, these authors also emphasized that there was considerable uncertainty in the radial wind field measurements, which the authors mention was the most important term in their budget analysis. Some of the first simulations used to infer the exchange coefficients were presented in Emanuel (1995). The results suggested that the ratio of the exchange coefficients was close to 1.5 in high wind conditions, however, if dissipative heating is taken into account, the ratio would be closer to unity (Bister and Emanuel 1998). Most subsequent formulations of the exchange coefficients exhibit a ratio close to this range, but there is not yet a firm consensus of how the exchange coefficients should scale with various meteorological variables. Emanuel (1995) noted that with relatively few observations at surface wind speeds exceeding 20 m s^{-1}, it was difficult to validate the results from the numerical simulations, particularly the predicted relationship between the ratio C_K/C_D and the maximum azimuthal wind speed. The sensitivity of TC intensity to C_K and C_D from the theoretical analysis in Emanuel (1986) and Emanuel (1995) coupled with the challenges associated with estimating their values that these early studies discussed precipitated a vigorous pursuit of more accurate formulations for the exchange coefficients.

b. *Hypothesizing scaling laws for the high wind regime: Emanuel (2003)*

A set of scaling laws was developed in Emanuel (2003, hereafter E3) suggesting that at very high wind speeds the surface exchange coefficients become independent of wind speed, but may depend on temperature. E3 considered an idealized setup to isolate the key meteorological variables that control air–sea flux in the presence of ubiquitous spray and high winds. The setup was an interface between semi-infinite regions of water and air with a uniform, horizontal pressure gradient applied in the air. At high wind speeds there is no clearly defined interface, but rather a continuum between bubble-filled water and spray-filled air. The essential parameters which govern this system are assembled into three dimensionless numbers:

$$R_u \equiv \frac{\rho_l u_*^4}{\sigma g'}, \quad R_\sigma \equiv \frac{\sigma}{\rho_l \upsilon_l^{4/3} g'^{1/3}}, \quad R_\upsilon \equiv \frac{\upsilon_l}{\upsilon_a},$$

where ρ_l is the density of water, σ is surface tension, g' is reduced gravity, υ_l is the kinematic viscosity of water, and υ_a is the kinematic viscosity of air. Since R_σ and R_υ are constants, the dynamics of a particular system can only scale with R_u. E3 hypothesized that there is a regime of R_u corresponding to very high wind speeds where the system dynamics become independent from R_u. Additionally, the only length scale that remains independent of viscous parameters is the Charnock length $l_c = u_*^2/g'$ (Charnock 1955). This implies that any other length scales that might grow with wind speed, like the depth of the spray layer, must be a function of the Charnock length. E3 used a mechanistic argument to show that the ratio C_K/C_D is independent of wind speed and a decreasing function of the undisturbed air temperature. This argument related the upward mass flux of spray to both the air–sea enthalpy flux and the air–sea momentum flux, resulting in a ratio C_K/C_D that is close to unity for typical TC conditions. The similarity hypothesis predicts a wind regime transition such that low wind speed surface fluxes cannot be accurately extrapolated beyond the transition point, and the numerical experiments that tested the hypothesis in the last section of E3 used a gradient wind speed of 30 m s^{-1} as the transition point. The sea surface transition around wind speeds of 30 m s^{-1} is one of the recurring results across many subsequent studies.

3. Estimating C_K and C_D from in situ observations

The Coupled Boundary Layer Air–Sea Transfer (CBLAST) experiment was a collaboration between several divisions of the National Oceanic and Atmospheric Administration and the Office of Naval Research that diagnosed air–sea interaction with many different techniques in a variety of environments from 2000 through 2005 (Black et al. 2007). One of the goals of the experiment was to study air–sea interaction in TCs so that parameterizations of boundary layer exchanges, and ultimately intensity forecasts, could be improved. The in situ data collected from airborne radar, GPS dropsondes, and ocean buoys during this experiment represented the first measurements relevant to air–sea flux at 10-m wind speeds above 22 m s^{-1}. The momentum flux was calculated from both flight level measurements (French et al. 2007) and ocean buoys (Jarosz et al. 2007). Both studies found that the drag coefficient increased and then decreased with wind speed, although the peak C_D occurred at slightly different values of U_{10}, about 25 m s^{-1} for French et al. (2007) and about 32 m s^{-1} for Jarosz et al. (2007). The results from Jarosz et al. (2007) were shown to be very similar to those from a much more recent study by Zou et al. (2018) that also used ocean buoy data to estimate the drag coefficient. The first direct measurements of latent heat flux from the hurricane boundary layer were published by Drennan et al. (2007); profiles of specific humidity, potential temperature, and wind speed are shown in Fig. 4 of their paper. They found that the Dalton number, or humidity flux coefficient, exhibited no significant wind speed dependence for 10-m wind speeds up to 30 m s^{-1} and had an average value of 1.18×10^{-3}. Zhang et al. (2008) published the first direct observations of sensible heat flux for 10-m wind speeds up to 30 m s^{-1} and calculated the enthalpy flux coefficient. The average C_K from their measurements was $(1.16 \pm 0.07) \times 10^{-3}$, and their results did not show a detectable wind speed dependence for C_K. They suggested that surface conditions including sea spray, may be responsible for the observed, nearly constant result. Bell et al. (2012) estimated C_D and C_K by using a control volume approach and also did not find a strong wind speed dependence in either coefficient

or their ratio, although their estimates have very large error bars.

Several studies have examined GPS sonde profiles from TCs in order to estimate C_D and C_K from classical flux-profile relationships, and concluded that the sea spray and foam at the surface significantly modulate the air–sea fluxes. Powell et al. (2003) published the first estimates of C_D in a TC using GPS sonde data. Their analysis showed that the mean wind profile was very nearly logarithmic with height, in agreement with Eq. (3), and the calculations of C_D suggested that the sea surface drag coefficient peaked near $U_{10} = 40\,\mathrm{m\,s^{-1}}$. Holthuijsen et al. (2012) similarly analyzed GPS sonde data to estimate the drag coefficient, though they used many more profiles and showed results for C_D over a larger range of wind speeds. Holthuijsen et al. (2012) used an iterative approach based on a modified neutral stability wind profile from Vickery et al. (2009) to calculate the roughness length, and estimated the fraction of white-cap coverage from the wind speed. Using azimuthally averaged winds, they also found that the drag coefficient peaked around $U_{10} = 40\,\mathrm{m\,s^{-1}}$, which was the same wind speed at which the whitecap fraction reached 100%. When they calculated the drag coefficient separately for different regions, they found C_D varied in azimuth. Specifically, the cross-swell region, which starts from the TC translation vector and continues cyclonically for approximately 120°, exhibited a larger drag coefficient for $U_{10} > 30\,\mathrm{m\,s^{-1}}$. Both studies suggested that the prevalence of spray and foam at higher wind speeds was responsible for lowering the sea surface drag by creating a ''slip'' layer. Laboratory experiments which support these findings are discussed in section 4 of this review. Richter and Stern (2014) used sonde profiles to specifically look for evidence of sea spray–mediated enthalpy flux. They found values of C_K that were generally within the range of values from other sources, but noted that the scaling of the computed enthalpy flux H_K much more closely followed the scaling of spray-mediated fluxes with wind speed than the scaling of interfacial fluxes with wind speed from Andreas et al. (2008). Richter and Stern (2014) hypothesized that one of the reasons for the discrepancy between the estimates of C_K from laboratory studies and in situ measurements is that laboratory studies may be primarily detecting the interfacial enthalpy flux. Richter and Stern (2014) concluded that not only do observations appear to be detecting spray fluxes, but the observed scaling suggested that sea spray is the dominant mechanism for air–sea enthalpy flux in TCs.

Richter et al. (2016) investigated how precisely the flux-profile method, used by several studies including Powell et al. (2003) and Holthuijsen et al. (2012), can estimate either C_K or C_D. The flux-profile method relies on Monin–Obukhov similarity theory and the assumption of neutral stability which results in the wind profile from Eq. (3). Richter et al. (2016) analyzed sonde data and the results from a large-eddy simulation in which the exchange coefficients were prescribed. The findings suggested that the flux-profile method can be useful for diagnosing general trends in the exchange coefficients as functions of wind speed, but the method may result in relative errors as large as 50% for C_D and 200% for C_K for 10-m wind speeds up to $50\,\mathrm{m\,s^{-1}}$. This study identified two types of factors that contribute to uncertainty in the calculation of the exchange coefficients: ''internal'' factors which are parameters specific to the flux-profile method like the bin width used to group sonde profiles by velocity, and ''external'' factors like uncertainty in the sea surface temperature or potential violations of the neutral stability assumption in the near-eyewall region.

A few theoretical models used a turbulent kinetic energy budget of the spray layer to explain the apparent decrease or leveling-off of drag at high wind speeds from in situ observations. Makin (2005) used the logarithmic solution to the turbulent kinetic energy balance equation from Barenblatt (1979), who considered a turbulent region laden with heavy particles, to develop a resistance law for the sea surface drag in the presence of a stable layer of suspended sea spray drops. The solution of the resistance law, which is applicable only in the presence of substantial spray production corresponding to $U_{10} \geq 33\,\mathrm{m\,s^{-1}}$, indicates that the drag coefficient gradually levels off, in agreement with Powell et al. (2003). Kudryavtsev (2006) found that the layer of large, heavy spume drops produced at high wind speeds inhibited turbulent mixing and led to a decrease of the drag coefficient starting around $U_{10} = 20\,\mathrm{m\,s^{-1}}$ and continuing through the highest wind speeds considered of almost $U_{10} = 80\,\mathrm{m\,s^{-1}}$, where the drag coefficient dropped to nearly 1.0×10^{-4}. This apparent ''slippery surface'' at high wind speeds also agreed well with Powell et al. (2003). Bianco et al. (2011) constructed a budget of turbulent kinetic energy for the spray-filled marine surface boundary layer. The authors designed exchange coefficient formulations from the results of several earlier studies (Fairall et al. 1996; Powell et al. 2003; Black et al. 2007; Zhang et al. 2008) such that their C_D peaked around $U_{10} = 30\,\mathrm{m\,s^{-1}}$ while C_K monotonically increased. Their model showed that the larger drop sizes produced by higher wind speeds helped stabilize the spray layer, which led to both a decrease in drag and an increase in sensible and latent heat fluxes. They tested their parameterization of sea spray in the Weather Research and Forecasting (WRF) Model (Skamarock et al. 2008) and found that including sea spray led to a substantial increase TC intensity compared to a control run.

4. Estimating C_K and C_D from laboratory experiments

A series of experiments with the University of Miami Air–Sea Interaction Saltwater Tank (ASIST) represented some of the first laboratory tests aimed at measuring the air–sea enthalpy and momentum fluxes under high wind conditions. The wave tank has a 1-m^2 cross section and a 15-m-long experimental section. Donelan et al. (2004) used an x-film anemometer to directly measure the Reynolds stress; the results from these experiments showed that the drag coefficient appeared to increase with wind speed initially and then remain relatively constant. Curcic and Haus (2020) discovered a postprocessing error that did not affect the overall profile from Donelan et al. (2004), but did somewhat alter the magnitude of the drag coefficient and the wind speed at which it appeared to saturate. After the correction, the results from Donelan et al. (2004) showed C_D increased from about 1.5×10^{-3} to about

3.0×10^{-3} for 10-m wind speeds from 5 to 30 m s^{-1} and did not increase much beyond 3.0×10^{-3} for 10-m wind speeds between 30 and 45 m s^{-1}. Haus et al. (2010) replicated the experiments from Donelan et al. (2004) to calculate the drag coefficient and also collected detailed temperature observations to calculate C_K. The results suggested C_K is relatively constant near 1.0×10^{-3} for moderate 10-m wind speeds between 5 and 35 m s^{-1}, which results in the ratio C_K/C_D fluctuating between 2 and 0.5 over the same wind speeds. Jeong et al. (2012) used ASIST experiments to estimate C_K and calculated that sea spray was enhancing C_K by at most 38% compared to spray-free conditions. This capacity to increase in the transfer coefficient did not appear to vary with the 10-m wind speed as long as it was above 13 m s^{-1}. The calculated C_K values from these experiments were consistent with those in Haus et al. (2010). Curcic and Haus (2020) also conducted experiments with the ASIST setup similar to those of Donelan et al. (2004). Their results agreed well with previous experiments; the calculated C_D saturated close to 2.5×10^{-3} after the 10-m wind speed exceeded about 25 m s^{-1}. A couple of studies, Soloviev et al. (2014) and Soloviev et al. (2017), used results from ASIST experiments along with companion numerical experiments to explore how spume production at the air–sea interface could be thought of as resulting from Kelvin–Helmholtz instability at the surface. Their parameterization for C_D exhibited a peak near $U_{10} = 30$ m s^{-1} and an aerodynamic drag well near $U_{10} = 60$ m s^{-1}. These findings suggested that between $U_{10} = 30$ m s^{-1} and $U_{10} = 60$ m s^{-1}, conditions at the sea surface favor intensification since C_D decreases with increasing wind speed.

Komori et al. (2018) used wave tank experiments to separately measure the exchange coefficients for sensible heat C_H and latent heat C_E. The Kyoto University wave tank is 15 m long and has a cross section of 1.28 m^2. The bulk exchange parameterization from Eq. (1), which is used by many numerical models, assumes that $C_H = C_E = C_K$. Komori et al. (2018) was the first study to test whether this assumption was valid in the high wind regime. The results from the laboratory experiments, which tested a range of equivalent 10-m wind speeds up to $U_{10} = 60$ m s^{-1}, showed that C_H and C_E are very nearly equal to C_K for the high wind regime. All three exchange coefficients also appear to be nearly constant with wind speed until a significant amount of spray and foam is produced at about $U_{10} = 35$ m s^{-1}. The authors also computed C_D from their experimental results and found that C_D increased until about $U_{10} = 35$ m s^{-1} after which point the coefficient appeared to remain constant. The ratio of C_K/C_D from these results is slightly larger than other estimates reaching above 1.25 for $U_{10} = 80$ m s^{-1} as shown in Fig. 3.

Troitskaya et al. (2020) analyzed the data from two wave tank experiments to study the effect of surface waves on the bulk exchange coefficients. The experiments used for this analysis included Komori et al. (2018) and experiments conducted in the Large Thermally Stratified Tank (LTST) at the Institute of Applied Physics Russian Academy of Sciences (IAP RAS); the facility for the latter is described in Troitskaya et al. (2012). The authors found that the drag coefficient gradually increased with both wind speed and wave fetch, while the heat exchange coefficient was relatively constant until approximately $U_{10} = 33$ m s^{-1}, where it increased steeply with increasing wind speed. The sharp increase in the heat transfer correlated with both the dominant wavelength increasing beyond 40 cm and with increased whitecapping.

While foam is routinely observed at the air–sea interface in high winds, experiments which measure its impact on surface fluxes are relatively recent. A few studies expected foam to play an important role in air–sea exchange. The concluding remarks of Emanuel (1995) suggested that surface exchange rates are likely sensitive to surfactants, and that the presence of either naturally occurring or man-made surfactants might be able to significantly modify the air–sea fluxes in TCs. As mentioned earlier, both Powell et al. (2003) and Holthuijsen et al. (2012) hypothesized that foam acted like a slip layer which worked to decrease the sea surface drag.

Troitskaya et al. (2019) studied the impact of foam that was naturally created through wave breaking and foam that was artificially created by introducing a surfactant in the LTST. The surfactant did not alter the surface tension or viscosity of the water and was able to generate substantial foam coverage. The quasi-linear framework described in Troitskaya et al. (2012) and Troitskaya et al. (2014) was used to calculate C_D from the experimental results. The quasi-linear model takes the roughness length as an input, so Troitskaya et al. (2019) developed a new model of the roughness length to account for a sea surface with foam. Some aspects of this roughness length model are similar to the model of roughness length from Golbraikh and Shtemler (2016). Troitskaya et al. (2019) found that the drag coefficient increased with the mean square slope of the surface, and that the mean square slope decreased as the fraction of the surface covered with foam increased. In other words, more foam coverage tended to lower the steepness of the surface, and the less steep the surface the smaller the drag coefficient was found to be. Troitskaya et al. (2019) also offered an explanation for why the calculated drag coefficient from both their analysis and from many others who also considered foam-covered surfaces [e.g., Powell et al. (2003), Jarosz et al. (2007), Holthuijsen et al. (2012) and Richter et al. (2016), who used in situ measurements, or Golbraikh and Shtemler (2016) and Golbraikh and Shtemler (2020), who used laboratory measurements] increases with U_{10} until a wind speed of about 30 m s^{-1}, after which point it appears to decrease. At lower wind speeds, there is little foam coverage and so as the wind speed increases the steepness of the surface increases and the production of spray, which serves as a momentum sink, increases. Both of these effects contribute to increased drag. However, at higher wind speeds where there is substantial foam coverage, there are many competing effects which together result in a net decrease of the drag. Troitskaya et al. (2019) identified two processes in the high wind speed regime that increased the surface stress; these are an observed widening of the wave frequency spectrum and an increase in the number of spray-producing events as described in Troitskaya et al. (2017) and Troitskaya et al. (2018b). Three high wind speed regime processes that decreased in drag, and ultimately overwhelm the previous two processes, include an increase in the fractional foam coverage, a decrease in the size of foam

bubbles, and a decrease in the size and duration of spray-producing events.

Vanderplow et al. (2020) also conducted laboratory experiments to estimate the influence of surfactants, but they were specifically interested in how biosurfactants could modify the sea spray generation function. The experiments were conducted with the previously mentioned ASIST setup. The laboratory results, which were validated with numerical experiments, showed that the concentration of spray drops with radii between 100 and 500 μm increased by approximately 39% in the presence of surfactants. This suggested that regions affected by algal blooms or oil spills may locally exhibit more sea spray and modify TC intensity. However, since more sea spray could both enhance the enthalpy flux and increase the sea surface drag, it is difficult to generalize about the effect that surfactants have on TC intensity.

5. The Andreas corpus

The series of publications by Edgar Andreas on this topic is almost a guided tour of the developments in sea spray–mediated fluxes over the last 30 years.

The phase change equations developed by the cloud microphysics community were the foundation of Andreas's microphysical model. He began with the coupled system of equations in Pruppacher and Klett (1978), which described the evolution of the temperature and radius of a single drop suspended in uniform air. The change in a drop's temperature and radius, for a given set of ambient meteorological conditions, can be used to calculate the enthalpy exchange between a drop and the atmosphere according to the model described throughout Andreas (1989, 1990, 1992, 1995) and AE1. Under the two assumptions that all of the sea spray is able to cool to at least the ambient air temperature, and all of the spray which reenters the sea does so at the wet bulb temperature T_w, the total sea spray enthalpy flux $Q_{k,\mathrm{sp}}$ is

$$Q_{k,\mathrm{sp}} = \rho_l c_w [T_s - T_a + f(T_a - T_w)]F, \tag{4}$$

where c_w is the specific heat of seawater, T_s is the sea surface temperature, T_a is the ambient air temperature, f is the fraction of sea spray that falls back to the sea, and F is the total sea spray volume flux.

Andreas defined characteristic time scales over which individual spray drops exchanged enthalpy and momentum with the atmosphere, and these time scales have since been used by many, if not most, subsequent studies of sea spray flux. The four main time scales are τ_T, τ_r, τ_f, and τ_{ac}. The two time scales τ_T and τ_r correspond to the time when the drop is within one e-folding fraction of its equilibrium wet bulb temperature T_{eq} and equilibrium radius r_{eq}, respectively (Andreas 1990, 1995). Several papers, including Andreas (1995) and AE1, compared these two time scales to illustrate the temporal decoupling between the relatively fast process of temperature equilibration and the relatively slow process of mass loss. AE1 showed that a drop that reenters the sea right after the fast process of temperature adjustment has finished can substantially enhance the air–sea enthalpy flux. This is discussed in detail below. Andreas (2005) discussed how these two time constants, along with T_{eq} and r_{eq} can be estimated without integrating the fully coupled evaporation equations from Pruppacher and Klett (1978). The last two time scales τ_f and τ_{ac} correspond to the time a drop spends aloft before reentering the sea and the time it takes for a drop to accelerate to within one e-folding fraction of U_{10} (Andreas 1992, 2004). A drop will transfer the most enthalpy when τ_f is both greater than τ_T and much less than τ_r. Additionally, a drop will extract the maximum amount of momentum when $\tau_{\mathrm{ac}} \ll \tau_f$.

AE1 studied the impact of sea spray–mediated fluxes on the large-scale enthalpy and momentum fluxes in tropical cyclones. While several earlier studies used the microphysics of sea spray evaporation to estimate the contribution of sea spray to the large-scale air–sea fluxes at low wind speeds (Rouault et al. 1991; Fairall et al. 1994; Andreas et al. 1995), AE1 explored how sea spray evaporation could substantially enhance the enthalpy flux in the boundary layer of tropical cyclones where sea spray is ubiquitous. AE1 attributed an enhanced enthalpy flux to reentrant sea spray, which is sea spray that only partially evaporates before returning to the sea. After ejection, a drop will rapidly cool to its wet bulb temperature while it loses only about 1% of its mass (Andreas 1995), then the drop will steadily warm and shrink, exchanging sensible for latent heat with the air until the drop is in thermoequilibrium with the local air temperature. The drop contributes the maximum amount of enthalpy to the air when it returns to the sea just after it reaches its wet bulb temperature, which is lower than the ambient air temperature and also the coldest the drop gets during its life cycle. Further evaporation will reduce the mass of the drop without lowering its temperature, thereby reducing its net enthalpy transport. The total spray-mediated enthalpy flux was calculated from an enthalpy conservation budget, although it is also possible to derive the enthalpy flux from the microphysical evaporation equations, as was done in Troitskaya et al. (2018b). The size of the spray drop is very important in this analysis. Smaller drops, with radii on the order of 10 μm, are very likely to evaporate completely before reentering the sea, contributing little to the total enthalpy flux. AE1 suggested that large drops, with radii on the order of 500 μm, are unlikely to remain aloft long enough to contribute substantially to the enthalpy flux. The drop size used as a proxy for all sea spray in this analysis is the 100-μm drop, which is likely to return to the sea about 3 K colder than the ambient air temperature for typical TC surface conditions. The results showed that the enthalpy flux from sea spray was about 79 W m^{-2} under moderate wind speeds of $U_{10} \approx 20$ m s^{-1}, and is likely substantially larger for higher wind speeds which produce more spray.

Both AE1 and Andreas (2004) estimated the sea spray–mediated momentum flux, or spray stress, from the amount of energy needed to accelerate the spray drops. All drops except the very largest ones were assumed to reach a significant fraction of the free stream velocity. The largest drops are not necessarily negligible, even if they are only aloft for a short time, since they are the most massive and take the most energy to accelerate. Note that any mass fluxed from sea to air, whether in the form of liquid or vapor, will accelerate toward the free stream velocity and thereby exert a drag on the air, and

in the case of spray drops this is true whether or not the drop reenters the sea. On the other hand, the stress on the ocean exerted by spray is exclusively owing to reentrant drops.

Andreas considered the total air–sea enthalpy and momentum fluxes to be the sum of an interfacial flux and a spray flux. Andreas et al. (2008) described how these two pathways scale differently with mean meteorological variables such as wind speed, air–sea temperature difference, and the gradient of specific humidity. For instance, the interfacial enthalpy flux appears to scale linearly with wind speed while the spray enthalpy flux appears to scale at a rate greater than quadratic with wind speed. This difference in scaling was later leveraged by Richter and Stern (2014) to identify the surface enthalpy flux source from observations. The momentum flux is also expected to scale differently according to AE1, who showed that the interfacial momentum flux scales with u_*^2 while the spray momentum flux scales with u_*^4. Andreas (2004) estimated that for low wind conditions ($U_{10} < 30\,\mathrm{m\,s^{-1}}$), spray accounts for about 10% of the total surface stress while at high wind conditions ($U_{10} > 60\,\mathrm{m\,s^{-1}}$) spray accounts for nearly all of the stress.

The bulk flux COARE (Coupled Ocean–Atmosphere Response Experiment) algorithm is used to calculate the surface fluxes and the rate at which sea spray cools and salinates the sea surface; the evolution of this algorithm is described throughout Andreas et al. (2008), Andreas (2010), and Andreas et al. (2015). The COARE algorithm incorporated the results from several air–sea exchange studies as it evolved, most notably Fairall et al. (1996), Fairall et al. (2003), Perrie et al. (2005), and Andreas et al. (2012). The total enthalpy flux is modeled as the sum of interfacial and spray fluxes, and there is a feedback term that accounts for sea spray cooling the air just above the surface and increasing the air–sea temperature difference. The algorithm is constructed with three tuning parameters primarily to ameliorate the effect of uncertainty in the sea spray generation function. The sea spray generation function is the number of drops produced per unit area of sea surface, per unit time, per unit drop radius and is denoted dF/dr. The parameters are tuned with data from both HEXOS (Humidity Exchange Over the Sea; Katsaros et al. 1987; DeCosmo et al. 1996) and FASTEX (Fronts and Atlantic Storm-Tracks Experiment; Joly et al. 1997; Persson et al. 2005). Figures 5 and 7 of Andreas (2010) show that the amount by which sea spray can cool and salinate the sea surface increases with wind speed up to the lower bound of hurricane force winds ($U_{10} \approx 40\,\mathrm{m\,s^{-1}}$).

Andreas looked for evidence of sea spray–mediated flux in the data from both the HEXOS and the CBLAST (Coupled Boundary Layer Air-Sea Transfer; Black et al. 2007) experiments. Andreas and Decosmo (2001) analyzed data from the HEXOS experiment and found that the difference between the measured enthalpy flux and the enthalpy flux predicted by bulk aerodynamic models could be explained by a sea spray–mediated flux. Andreas and Decosmo (2001) used the HEXOS data to show that for moderate wind speeds of about 15–18 $\mathrm{m\,s^{-1}}$, sea spray supported between 10% and 40% of the total latent heat flux and about 10% of the total sensible heat flux, compared to the interfacial flux. Andreas (2010) later calculated, also using the HEXOS data, that the spray and interfacial fluxes contributed roughly equally to the total air–sea flux of enthalpy for wind speeds of about 40 $\mathrm{m\,s^{-1}}$. Andreas (2011) used the algorithm from Andreas et al. (2008) and Andreas (2010) to estimate C_K and C_D, or more precisely the neutral stability exchange coefficients that come from Eq. (3). The results showed that both C_K and C_D increased with wind speed, and both have values ranging from approximately 1.0×10^{-3} to about 4.0×10^{-3} for U_{10} from about 5 to 40 $\mathrm{m\,s^{-1}}$. The ratio C_K/C_D was between about 0.5 and 1.0 for this range of 10-m wind speeds, which was generally within the range of the data from CBLAST for the same wind speeds.

6. Numerical experiments

This section reviews the studies that used numerical simulations to estimate the sea spray fluxes. Many of the studies in this section considered an Eulerian carrier flow into which Lagrangian particles were injected, which is a much more computationally tractable way to estimate the influence of, and any feedbacks involving, sea spray compared to attempting to resolve microscale spray drop production processes.

The numerical model SeaCluse was among the earliest to model net sea spray–mediated fluxes from drop motions and concentrations. While SeaCluse was developed for 10-m wind speeds no greater than 25 $\mathrm{m\,s^{-1}}$ and only considered jet drops produced from bursting bubbles, these numerical experiments provided an important foundation and benchmark for subsequent numerical and theoretical investigations. SeaCluse is a 1D Eulerian model that treated drop mass concentrations as scalar fields in an approach similar to the one developed by Ling and Kao (1976). The drop mass concentrations are modulated by drop ejection, drop deposition, gravitational effects, inertial effects, turbulent diffusion, and evaporation. Model calibration was performed with results from experiments conducted in the Large Air–Sea Interaction Simulation Tunnel at Institut de Mecanique Statistique de la Turbulence through the HEXIST (HEXOS Experiments In the Simulation Tunnel) program, a component of the HEXOS program (Mestayer and Lefauconnier 1988; Mestayer et al. 1989). These experiments used submerged aerators to inject bubbles that would burst at the surface to produce jet drops. In one of its earliest iterations[1], Rouault et al. (1991) used the model to study the vertical profiles of drop mass concentrations, water vapor, and sensible heat under different humidity and wind speed conditions. As expected, a higher relative humidity generally suppressed evaporation. Of the two free-stream wind speeds considered 10 and 25 $\mathrm{m\,s^{-1}}$, the higher wind speed condition led to three notable outcomes: 1) more vertically uniform mass concentrations, especially for larger drops, 2) a net greater water vapor flux from the same drop population, and 3) a corresponding net reduction in sensible heat flux. Mestayer et al. (1996) extended the code to model open ocean, rather than laboratory, conditions, although this version did

[1] This version of the model was called Couche Limite Unidimensionelle Stationnaire d'Embrums (CLUSE) which translates to one-dimensional, stationary, drop boundary layer.

not include evaporation. They found that drops tended to become concentrated near the wave crests, and were transported to this height primarily by the mean airflow between wave crests rather than by turbulent air motions. They also found that the residence time of larger drops ($r_0 > 90\,\mu$m) tended to be much less dependent on the 10-m wind speed than was predicted by Andreas (1992), increasing at a rate of $U_{10}^{0.3}$ rather than U_{10}^{2}. Van Eijk et al. (2001) incorporated evaporation into SeaCluse and, similar to the findings from Rouault et al. (1991), observed that water vapor flux from evaporating sea spray exhibited a strong wind speed dependence. At the highest wind speed examined $U_{10} = 20\,\mathrm{m\,s^{-1}}$, they found that the humidity exchange coefficient for the evaporating case was 30% larger than the nonevaporating case, underscoring the importance of sea spray–mediated water vapor flux.

Another early model, Gwaihir, was developed around the same time as SeaCluse and was also calibrated with data collected through the HEXIST program (Edson et al. 1988; Edson 1989; Edson and Fairall 1994; Edson et al. 1996). The simulations of evaporating drops in the 1D Lagrangian version of Gwaihir produced vertical profiles of liquid water content that agreed well with experimental results (Edson and Fairall 1994). Edson et al. (1996) combined the Lagrangian model with an Eulerian code, and allowed the drops to interact with the scalar fields of temperature and specific humidity. This extension improved the agreement between the numerical and experimental profiles of liquid water content compared to Edson and Fairall (1994). Additionally, the increase in the temperature and specific humidity fields due to drop evaporation under low wind speeds were shown to agree well with the results from Rouault et al. (1991). While they only considered a low wind speed of $U_{10} = 7.5\,\mathrm{m\,s^{-1}}$, Edson et al. (1996) found that drop evaporation effected maximum increases of 0.1°C and $0.05\,\mathrm{g\,kg^{-1}}$ in the temperature and specific humidity fields, respectively.

The series of papers describing the development of the Mueller–Veron model for air–sea flux from 2009 through 2014 culminated in estimates of how spray-mediated fluxes and bulk exchange coefficients evolved with wind speed. This model considered air–sea fluxes of momentum, sensible heat, and moisture to be the sum of the sea spray–mediated flux and the interfacial flux. The interfacial momentum flux is calculated according to the model described in Mueller and Veron (2009c) and the interfacial sensible heat and moisture fluxes are calculated according to the model described in Mueller and Veron (2010b). Mueller and Veron (2014a) used a Lagrangian stochastic model of evaporating sea spray drops, the development of which is described in Mueller and Veron (2009b) and Mueller and Veron (2010a), to estimate the contributions from individual drops to the overall flux. In contrast to Andreas (1992), which considered drop residence times to depend on the significant wave height, the results from Mueller and Veron (2014a) did not show a clear relationship between the residence times and the significant wave height. The results showed that small drops (defined as drops whose terminal velocity was less than the vertical turbulent velocity) in particular reentered the sea much warmer than predicted by the microphysical equations for a drop experiencing the ambient 10-m conditions. The explanation was that the adjustment time scales for small drops is sufficiently short that, even if they experienced ambient conditions at 10 m during their flight, the drops warm up before reentry as they adjust to the near-surface conditions. This has the effect of depressing the net sensible heat flux. Mueller and Veron (2014b) developed a feedback model that used the final temperatures and radii of spray from the Lagrangian stochastic simulations in Mueller and Veron (2014a). The sea spray generation functions from both Fairall et al. (1994) and Mueller and Veron (2009a) were used to study how the composition of spray affects the fluxes. Mueller and Veron (2014b) found that the sea spray mediated no more than about 10% of the total momentum flux for either sea spray generation function (SSGF) at any wind speed up to $U_{10} = 50\,\mathrm{m\,s^{-1}}$, in contrast to Andreas (2004) which found that by $U_{10} = 60\,\mathrm{m\,s^{-1}}$, spray mediated nearly all of the momentum flux. The feedback model allows spray fluxes to modify the ambient conditions, which in turn affects the spray fluxes. Figure 6 of Mueller and Veron (2014b) shows the impact of feedback effect on the spray-mediated fluxes of sensible and latent heat; the results highlight the sensitivity of spray-mediated fluxes to the SSGF. While using the feedback model at higher wind speeds generally resulted in less spray-mediated sensible and latent heat flux for the SSGF from Fairall et al. (1994), the same could not be said of the SSGF from Mueller and Veron (2009a). Using the latter SSGF resulted in a slight flux enhancement at $U_{10} = 50\,\mathrm{m\,s^{-1}}$. Finally, the drag coefficient calculated from these results using either SSGF agreed well with previous estimates; C_D increased relatively steeply with wind speed until about $U_{10} = 30\,\mathrm{m\,s^{-1}}$ and subsequently increased more slowly with wind speed. The enthalpy exchange coefficient also agreed well with previous estimates, most of which corresponded to wind speeds below $U_{10} = 30\,\mathrm{m\,s^{-1}}$. At higher wind speeds, their estimate of C_K increases sharply in agreement with some more recently published coefficients from Troitskaya et al. (2018b) and Komori et al. (2018).

Lagrangian spray particles subject to large eddy circulations in the boundary layer of a TC were analyzed throughout Shpund et al. (2011, 2012) and Shpund et al. (2014). The domain was a 2D r–z plane that extended 600 m in the radial direction and 400 m in the vertical from the ocean surface. The simulation explicitly calculated the sea spray dynamics including the growth, condensation, evaporation, sedimentation, and collisions of drops. Shpund et al. (2011) found that the large eddy-driven enthalpy flux increased with the background wind speed for wind speeds up to $U_{10} = 20\,\mathrm{m\,s^{-1}}$. Shpund et al. (2012) found that sea spray evaporation moistens and cools the boundary layer when the relative humidity is below 90% while evaporation is significantly inhibited at humidities much higher than 90%. Shpund et al. (2014) found that spray contributed up to a 15% increase in relative humidity and up to a 1.5-K temperature drop in the simulation domain as the 2D region translated radially from the eye toward the eyewall. Shpund et al. (2014) concluded by proposing a new sea spray drop size distribution based on their simulation results.

The three studies Peng and Richter (2017, 2019) and Peng and Richter (2020) used direct numerical simulations (DNSs) with a Lagrangian–Eulerian framework and focused on whether common assumptions made by many bulk flux algorithms, including

neglecting interactions between spray drops and neglecting feedbacks between spray fluxes and the ambient conditions, are valid assumptions. The 3D domains used throughout these experiments were all on the order of 0.01 m^3, had a no slip lower boundary condition, and a stress-free upper boundary condition. The friction Reynolds numbers for the experiments ranged from 200 to 1500. Spray particles were injected at random locations on the lower boundary with an initial velocity that was randomly chosen from a uniform distribution between zero and the velocity that would propel the drop to 1/8 of the domain height in quiescent conditions. For each particle that exited the domain, another was injected such that the number of particles was constant. The model allowed the spray to exchange momentum, heat, and moisture with the ambient environment. Sea spray exchanged momentum with the air through the particle momentum equation which had both a Stokes drag and a gravitational settling term. Sea spray exchanged heat and moisture with the air according to the thermodynamic flux model based on the formulations from Andreas (1992, 1995); Mueller and Veron (2010a) and Helgans and Richter (2016). The results from Peng and Richter (2017) showed that small drops with radii less than 50 μm were not able to contribute much enthalpy flux, while larger drops could enhance the enthalpy flux. This agrees well with the drop size analysis in AE1. The results from Peng and Richter (2019) suggested that bulk flux formulations, specifically those from Fairall et al. (1994) and Andreas et al. (2015), may overestimate the contribution from sea spray. Peng and Richter (2019) found that the Andreas et al. (2015) formulation may overestimate the sensible heat flux from sea spray by as much as an order of magnitude and that the Fairall et al. (1994) formulation resulted in total fluxes that are up to 120% of the total fluxes computed by the DNS for small ($r < 20\,\mu$m) drops, but was generally more accurate for larger ($r > 70\,\mu$m) drops. One of the reasons for this was that the DNS results showed that there was a negative feedback between the interfacial flux of heat and the spray flux of heat, which is in contrast to the bulk flux formulation from Andreas et al. (2015) that assumed a positive feedback between interfacial and spray fluxes. Another reason the two bulk parameterizations considered here may overestimate the enthalpy flux compared to the DNS results is that they assumed that spray drops experience the ambient 10-m conditions and generally return to the sea after they have cooled substantially, but before the drop lost much mass. The DNS showed that drops with long residence times relative to their thermal adjustment time scale typically do not reenter much cooler than the ambient air temperature. The smaller a drop is, the longer its residence time, and the more likely it is that the bulk formulations will consider it to have contributed more enthalpy than these DNS results predict. The authors suggested a technique for mitigating overestimations from drops which are aloft longer could be to calculate an effective ambient environment that is a function of the sea spray thermal and residence time scales. Unlike the previous two studies that used particles of the same radius in each experiment, and varied the size between experiments, Peng and Richter (2020) injected sea spray particles of different radii together to investigate the assumption that sea spray drops do not interact with each other. In particular, they studied whether it is accurate to superpose the fluxes from drops of different sizes as many bulk parameterizations do. The results from these DNSs suggested that spray drops of different sizes do interact. In one of these experiments, the error in the total heat flux was 15.5%, so neglecting to account for sea spray interactions could lead to a nontrivial overestimation of sea spray fluxes. One of the sources of error appeared to come from the large drops modifying the ambient environment in the near-surface region. As was found by other numerical experiments, the concentration of large drops was larger toward the bottom boundary compared to smaller drops which were more uniformly distributed throughout the domain. The small drops are very sensitive to the local air conditions near the bottom of the domain, as shown in Peng and Richter (2017), and so as the large drops contribute more latent heat to the near-surface region the contribution from the smaller drops is diminished according to the DNS. Since bulk parameterizations do not take this into account, they tend to overestimate the spray fluxes compared to the DNS results. To ameliorate the issue of flux overestimation due to the noninteraction assumption, the authors proposed selecting a representative drop in place of modeling the whole spectrum of drops, as is done in AE1, and suggested a volume-weighted approach for selecting the size of the drop. This simplifies the computational requirements of incorporating spray fluxes and the authors found that this approach worked well to avoid overestimating the spray fluxes.

7. Sea spray generation functions

Most if not all investigations that discuss the influence of sea spray on TC intensity raise the concern that significant uncertainty in the sea spray generation function (SSGF) is a primary obstacle inhibiting a more accurate estimate of air–sea exchange. While the amount of sea spray produced and the drop size distribution are critical for predicting the spray fluxes (Mueller and Veron 2014b), measuring sea spray production in high winds is exceptionally challenging and there are relatively few experiments which have attempted it.

The wealth of literature on the topic of sea spray production over the open ocean has motivated a number of studies to review and compare SSGFs. The sea spray aerosol community has contributed heavily to research on SSGFs, and particularly in quantifying the production of very small drops ($r < 10\,\mu$m). Reviews of work in this area can be found in Lewis et al. (2004), O'Dowd and De Leeuw (2007), and De Leeuw et al. (2011). Compared to these reviews, the reviews by Andreas (2002) and Veron (2015) include many more SSGFs that estimate spray production for relatively large drops ($r > 500\,\mu$m) under much higher wind speeds. The intention of this section is not to be a comprehensive review of SSGFs, but to highlight both the importance of and the challenges surrounding estimating the SSGF under extreme wind speeds.

Figure 4 shows a small subset of the SSGFs developed from observations. Since it is not possible to plot all of the functions for the same U_{10} due to either the limited wind speed range over which they were designed to be valid or due to the results coming from experiments that were conducted at only a few wind speeds, Fig. 4 separates the functions into a low wind speed group, evaluated at $U_{10} = 18\,\mathrm{m\,s^{-1}}$, and a high wind

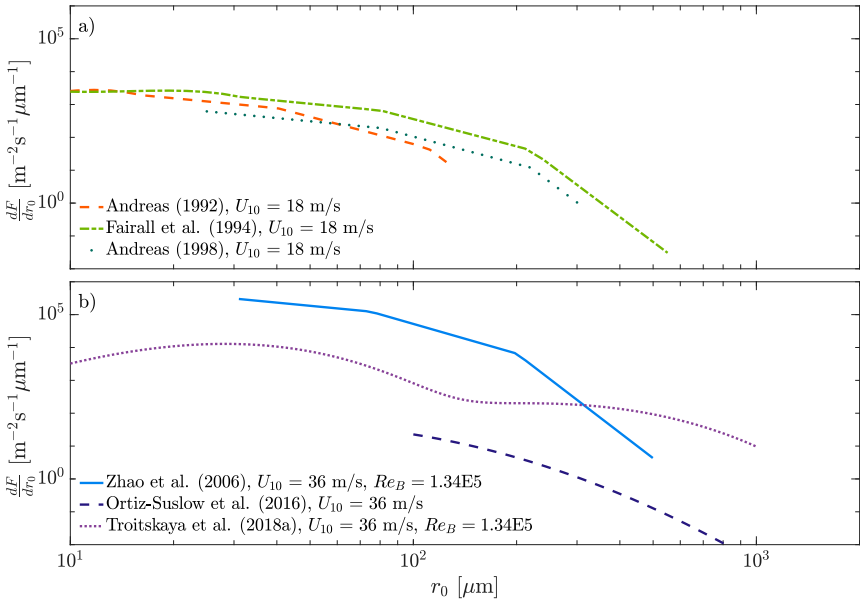

FIG. 4. A few of the available sea spray generation functions plotted as a function of initial drop radius r_0.

speed group, evaluated at $U_{10} = 36\,\mathrm{m\,s^{-1}}$. Initial estimates of spray generation at high wind speeds relied on extrapolating sparse observations from lower wind speeds. For example, Andreas (1992) developed an SSGF for moderate wind speeds of up to $U_{10} = 20\,\mathrm{m\,s^{-1}}$ based on observations from Wu et al. (1984), extrapolating the results to higher wind speeds and to larger drop sizes than were available in the data. Fairall et al. (1994) composed their SSGF by incorporating a whitecap fraction dependence from Fairall (1990) into the SSGF proposed by Andreas (1992). Andreas (1998) modified and extrapolated from the results in Smith et al. (1993) to arrive at a function that was valid for 10-m wind speeds up to $32.5\,\mathrm{m\,s^{-1}}$. Andreas (2002), who reviewed 13 SSGFs, concluded that the Fairall et al. (1994) SSGF was the most reliable to date.

The considerable discrepancies among the functions are themselves a topic of interest, and the subsequent studies offer several explanations of how differences in the wave-generation techniques, the composition of the water, the wave age parameter β, and the sea spray detection setup could affect the estimated SSGF.

Both of the studies by Fairall et al. (2009) and Ortiz-Suslow et al. (2016) generated spume in a wave tank and then used a profile-matching technique to estimate the SSGF. Fairall et al. (2009) concluded that the observed concentration of drops agreed well with the theoretical power-law concentration profile, while Ortiz-Suslow et al. (2016) found that a logarithmic concentration profile better fit the observed concentrations in their experiments than the more commonly used power-law profile. These experiments differed slightly in the way they produced waves which may have led to differences in spray production; Ortiz-Suslow et al. (2016) relied on wind alone while Fairall et al. (2009) used a combination of wind and a mechanical wave maker. Richter et al. (2019) conducted a large-eddy simulation of sea spray using Lagrangian particle tracking to evaluate the technique of profile-matching, which is predicated on reaching an equilibrium state where drop generation balances drop deposition. The results from Richter et al. (2019) showed that the profile-matching technique does not work well for large drops (with radii greater than about 600 μm) since they are likely to be significantly impacted by near-surface wave-induced turbulence and to have enough mass such that their trajectories deviate from the streamlines of the flow. Figure 4 of Richter et al. (2019) shows the discrepancy between the power-law prediction and the numerical simulation results for different drop sizes.

Mehta et al. (2019) used wave tank experiments to investigate the differences between freshwater spume and seawater spume. They found that using seawater led to more spume production at all measured radii ($86\,\mu\mathrm{m} \le r_0 \le 1386\,\mu\mathrm{m}$) and for all tested wind speeds ($36\,\mathrm{m\,s^{-1}} \le U_{10} \le 54\,\mathrm{m\,s^{-1}}$), but that seawater spume drops were generally more heavily concentrated near the lower levels while the freshwater drops were comparatively more evenly vertically dispersed. The authors compared their results to the wave tank experiments conducted by Fairall et al. (2009) and Veron et al. (2012). While Fairall et al. (2009) generally found lower concentrations of spray drops than Mehta et al. (2019) at similar wind speeds, there were some important differences between the two experiments. Fairall et al. (2009) may not have been able to measure large drops as well as Mehta et al. (2019) due differences in imaging equipment, the experiments made observations at different heights relative to the significant wave height, and Mehta et al. (2019) generated waves from wind alone rather than using the combination of wind and a wave maker. Fairall et al. (2009) also tested both fresh and saline water and did not find discrepancies as significant as those found by

Mehta et al. (2019), perhaps because Fairall et al. (2009) used salted freshwater (24 psu) while Mehta et al. (2019) used seawater (34 psu). The experimental setup of Mehta et al. (2019) was more similar to that of Veron et al. (2012), albeit Veron et al. (2012) only used freshwater. While Mehta et al. (2019) observed more large drops and fewer smaller drops than Veron et al. (2012), the results from the two freshwater experiments generally agreed well.

Several studies have adopted the dimensionless windsea Reynolds number as the independent parameter for their SSGFs rather than a wind speed variable; it has been shown to scale very well with measured spray production and greatly ameliorate large discrepancies in SSGF estimates. Toba and Koga (1986), and several subsequent studies that built on their work, showed that some surface processes, including the production of sea spray, scaled extremely well with the dimensionless number $\mathrm{Re}_B = u_*^2/(\omega_p \upsilon_a)$, where ω_p is the spectral peak frequency of the wind-waves (Iida et al. 1992; Zhao and Toba, 2001; Zhao et al. 2003). Named the windsea Reynolds number in Toba et al. (2006), Re_B describes the development of the sea surface and structure of the waves by comparing the inertial and viscous forces (Ma et al. 2020). As in Zhao et al. (2006), the windsea Reynolds number is often written as a product of $C_D U_{10}^3/(g\upsilon_a)$ and the wave age parameter $\beta = g/(\omega_p U_{10})$. Toba et al. (2006) showed that using Re_B as the independent variable produced much better agreement between estimates of C_D from different experiments than using either U_{10} or u_*, since C_D depends not only on the wind speed but also on the wave age. They also found that C_D generally increased with Re_B. Zhao et al. (2006) proposed a new SSGF that is a function of Re_B based on data from both laboratory experiments and field observations, and estimated the associated air–sea heat and momentum fluxes. Since Re_B considers both the wind speed and the development of the sea surface, it is especially helpful for comparing results from fetch-limited laboratory experiments with field observations. Zhao et al. (2006) found that the spray-induced stress, sensible heat flux, and latent heat flux all increased monotonically with Re_B; some notable regime transitions they observed include $\mathrm{Re}_B \approx 10^3$, which marks the appearance of spume, $\mathrm{Re}_B \approx 10^5$, which marks the point where spray heat fluxes are comparable to interfacial heat fluxes, and $\mathrm{Re}_B \approx 10^6$, which marks the point where spray momentum fluxes are comparable to interfacial momentum fluxes.

A series of laboratory experiments chronicled in Troitskaya et al. (2017, 2018a) and Troitskaya et al. (2018b) revealed how the production of large drops from an important sea spray creation mechanism had significant implications for both the structure of the SSGF under high wind conditions and the spray-mediated enthalpy and momentum fluxes. These experiments were conducted using the previously mentioned LTST (Troitskaya et al. 2012). The tank is 10 m long and has a cross-sectional area of 0.16 m^2. The equivalent 10-m wind speeds that were tested ranged from 18 to 33 $\mathrm{m\,s^{-1}}$. Troitskaya et al. (2017) showed that the dominant method of sea spray creation at high winds was the "bag-breakup" mechanism. This mechanism of spray production was first identified in wave tank experiments by Veron et al. (2012) who observed many more large spray drops than earlier SSGFs predicted (it is important to note that both the experiments in Veron et al. (2012) and the series of experiments by Troitskaya et al. were conducted with freshwater). Troitskaya et al. (2018a) meticulously explained how this mechanism increased the production of large spray drops. High-resolution images from the water's surface revealed bags, which have a thin membrane or canopy and a relatively thicker rim, would inflate and burst resulting in many small canopy drops and many large rim drops. This process results in a bimodal SSGF which is shown in Fig. 4; this SSGF is qualitatively similar to the drop size distribution published in Koga and Toba (1981) and Iida et al. (1992) where the authors hypothesized that two different processes were responsible for the separate peaks rather than two elements of one process. After quantifying the frequency of bag production under different wind and environmental conditions, Troitskaya et al. (2018a) found that the threshold for activating the bag-breakup mechanism in the laboratory was $\mathrm{Re}_B \approx 4000$ (corresponding to a 10-m wind speed of about 30 $\mathrm{m\,s^{-1}}$ in their setup). The authors also point out that with longer fetches, it may be possible that the threshold for bag-breakup becoming the dominant mechanism in field conditions could be closer to $U_{10} = 10\,\mathrm{m\,s^{-1}}$. Troitskaya et al. (2018b) quantifies the impact of this new SSGF on the air–sea flux of enthalpy and momentum, and proposed analytical functions for C_K and C_D based on these results, which are shown in Figs. 1 and 2. Both exchange coefficient formulations increase with U_{10} until about 30 $\mathrm{m\,s^{-1}}$, after which point the increase in C_K steepens while C_D stalls. As a result, the ratio of these coefficients C_K/C_D, which again is proportional to the square of the maximum potential intensity of TCs, also steepens around $U_{10} = 30\,\mathrm{m\,s^{-1}}$.

Impressive observations of the sea spray volume flux during Tropical Cyclone Olwyn were recently published by Ma et al. (2020). In situ observations of sea spray are incredibly sparse and rarely capture drops created in high wind speed conditions. Ma et al. (2020) used laser altimeters to observe the sea spray volume flux in 10-m wind speeds as high as 22.7 $\mathrm{m\,s^{-1}}$. The same instruments deployed for this field experiment were used to study sea spray production in a wave tank by Toffoli et al. (2011), the results of which generally agreed well with those of Troitskaya et al. (2018a) although, as in Ma et al. (2020), Toffoli et al. (2011) could only observe the total sea spray volume flux while Troitskaya et al. (2018a) observed the spray flux as a function of drop size. The observed sea spray volume flux from Ma et al. (2020) was two to three orders of magnitude larger than previous estimates from Iida et al. (1992), Fairall et al. (1994), Andreas (1998), Zhao et al. (2006), Toffoli et al. (2011), and Troitskaya et al. (2018a). The authors concluded by proposing a sea spray volume flux parameterization that is a function of both the windsea Reynolds number and the significant wave height.

8. Conclusions

Several studies have already integrated the findings from sea spray–mediated exchange into large-scale simulations. For example, Liu et al. (2011) simulated an idealized TC using WRF coupled to both a wave and an ocean model such that

spray fluxes and dissipative heating were able to influence the boundary layer energetics. They found a positive feedback between wind speed and the heat fluxes from spray and dissipative heating, which increased the maximum 10-m wind speed by about 20% compared to a control simulation. More recently, Garg et al. (2018) integrated spray-mediated flux formulations from the Andreas corpus along with surface-wave effects into WRF, and found that the spray and surface wave modules produced a stronger hurricane compared to a control simulation. Wada et al. (2018) showed that the choice of sea spray parameterization can significantly impact the air–sea latent heat flux in TC simulations. These findings support the conclusion that microscale processes can significantly influence large-scale dynamics, and demonstrate how improvements in sea spray flux parameterizations can be used to improve TC simulations.

While the values for C_K and C_D are well understood to an order of magnitude, their (often direct) proportionality to critical TC metrics represents a huge sensitivity that amplifies forecast uncertainty. Experiments can detect the influence of sea spray on the air–sea exchange and microphysical equations can be used to introduce the effects of sea spray into bulk parameterizations through C_K and C_D. Unfortunately, uncertainty in the SSGF ultimately propagates into the bulk formulations. However, theoretical and experimental efforts are converging on some common findings which are repeatedly corroborated through different techniques. For example, the qualitative nature of the sea surface appears to transition at a 10-m wind speed of about 30 m s^{-1}. Such a transition was predicted by the theoretical model in E3, supported by models like the one described in Andreas (2004), validated with observations of whitecap coverage (e.g., Holthuijsen et al. 2012) and laboratory experiments (e.g., Donelan et al. 2004), and coincides with the activation of a spray production mechanism that produces many more large drops that exert a greater influence on the surface fluxes compared to smaller drops (Troitskaya et al. 2018a). Both theoretical and experimental efforts confirm that sea spray has a significant effect on the total air–sea flux. Experimental data and theoretical models will continue to confirm and challenge existing preconceptions about the nature of sea spray and its role in modulating the intensity of tropical cyclones, working toward the common goal of improving intensity forecasts and our understanding of surface fluxes at extreme wind speeds.

Acknowledgments. This research was supported by Grant ICER-1854929 from the National Science Foundation.

Data availability statement. While this review does not include new data, the code used to produce the figures is available to anyone upon request.

REFERENCES

Andreas, E. L, 1989: Thermal and size evolution of sea spray droplets. Cold Regions Research Engineering Laboratory Tech. Rep. 89-11, 37 pp., https://ntrl.ntis.gov/NTRL/dashboard/searchResults/titleDetail/ADA210484.xhtml.

——, 1990: Time constants for the evolution of sea spray droplets. *Tellus*, **42B**, 481–497, https://doi.org/10.1034/j.1600-0889.1990.t01-3-00007.x.

——, 1992: Sea spray and the turbulent air-sea heat fluxes. *J. Geophys. Res.*, **97**, 11 429–11 441, https://doi.org/10.1029/92JC00876.

——, 1995: The temperature of evaporating sea spray droplets. *J. Atmos. Sci.*, **52**, 852–862, https://doi.org/10.1175/1520-0469(1995)052<0852:TTOESS>2.0.CO;2.

——, 1998: A new sea spray generation function for wind speeds up to 32 m s^{-1}. *J. Phys. Oceanogr.*, **28**, 2175–2184, https://doi.org/10.1175/1520-0485(1998)028<2175:ANSSGF>2.0.CO;2.

——, 2002: A review of the sea spray generation function for the open ocean. *Atmosphere-Ocean Interactions*, Vol. 1, W. A. Perrie, Ed., WIT Press, 1–46.

——, 2004: Spray stress revisited. *J. Phys. Oceanogr.*, **34**, 1429–1440, https://doi.org/10.1175/1520-0485(2004)034<1429:SSR>2.0.CO;2.

——, 2005: Approximation formulas for the microphysical properties of saline droplets. *Atmos. Res.*, **75**, 323–345, https://doi.org/10.1016/j.atmosres.2005.02.001.

——, 2010: Spray-mediated enthalpy flux to the atmosphere and salt flux to the ocean in high winds. *J. Phys. Oceanogr.*, **40**, 608–619, https://doi.org/10.1175/2009JPO4232.1.

——, 2011: Fallacies of the enthalpy transfer coefficient over the ocean in high winds. *J. Atmos. Sci.*, **68**, 1435–1445, https://doi.org/10.1175/2011JAS3714.1.

——, and J. Decosmo, 2001: The signature of sea spray in the HEXOS turbulent heat flux data. *Bound.-Layer Meteor.*, **103**, 303–333, https://doi.org/10.1023/A:1014564513650.

——, and K. Emanuel, 2001: Effects of sea spray on tropical cyclone intensity. *J. Atmos. Sci.*, **58**, 3741–3751, https://doi.org/10.1175/1520-0469(2001)058<3741:EOSSOT>2.0.CO;2.

——, J. B. Edson, E. C. Monahan, M. P. Rouault, and S. D. Smith, 1995: The spray contribution to net evaporation from the sea: A review of recent progress. *Bound.-Layer Meteor.*, **72**, 3–52, https://doi.org/10.1007/BF00712389.

——, P. O. G. Persson, and J. E. Hare, 2008: A bulk turbulent air–sea flux algorithm for high-wind, spray conditions. *J. Phys. Oceanogr.*, **38**, 1581–1596, https://doi.org/10.1175/2007JPO3813.1.

——, L. Mahrt, and D. Vickers, 2012: A new drag relation for aerodynamically rough flow over the ocean. *J. Atmos. Sci.*, **69**, 2520–2537, https://doi.org/10.1175/JAS-D-11-0312.1.

——, ——, and ——, 2015: An improved bulk air–sea surface flux algorithm, including spray-mediated transfer. *Quart. J. Roy. Meteor. Soc.*, **141**, 642–654, https://doi.org/10.1002/qj.2424.

Barenblatt, G., 1979: *Similarity, Self-Similarity, and Intermediate Asymptotics*. Consultants Bureau Plenum Press, 218 pp.

Bell, M. M., M. T. Montgomery, and K. A. Emanuel, 2012: Air–sea enthalpy and momentum exchange at major hurricane wind speeds observed during CBLAST. *J. Atmos. Sci.*, **69**, 3197–3222, https://doi.org/10.1175/JAS-D-11-0276.1.

Bianco, L., J.-W. Bao, C. W. Fairall, and S. A. Michelson, 2011: Impact of sea-spray on the atmospheric surface layer. *Bound.-Layer Meteor.*, **140**, 361, https://doi.org/10.1007/s10546-011-9617-1.

Bister, M., and K. A. Emanuel, 1998: Dissipative heating and hurricane intensity. *Meteor. Atmos. Phys.*, **240**, 233–240, https://doi.org/10.1007/BF01030791.

Black, P. G., and Coauthors, 2007: Air–sea exchange in hurricanes: Synthesis of observations from the Coupled Boundary Layer Air–Sea Transfer Experiment. *Bull. Amer. Meteor. Soc.*, **88**, 357–374, https://doi.org/10.1175/BAMS-88-3-357.

Bortkovskii, R. S., 1987: *Air-Sea Exchange of Heat and Moisture during Storms*. Springer, 192 pp.

Bryant, K. M., and M. Akbar, 2016: An exploration of wind stress calculation techniques in hurricane storm surge modeling. *J. Mar. Sci. Eng.*, **4**, 58, https://doi.org/10.3390/jmse4030058.

Byers, H., 1944: Atmospheric turbulence and the wind structure near the surface of the Earth. *General Meteorology*, McGraw-Hill, Ch. XXIV.

Charnock, H., 1955: Wind stress on a water surface. *Quart. J. Roy. Meteor. Soc.*, **81**, 639–640, https://doi.org/10.1002/qj.49708135027.

Chen, Y., F. Zhang, B. W. Green, and X. Yu, 2018: Impacts of ocean cooling and reduced wind drag on Hurricane Katrina (2005) based on numerical simulations. *Mon. Wea. Rev.*, **146**, 287–306, https://doi.org/10.1175/MWR-D-17-0170.1.

Curcic, M., and B. K. Haus, 2020: Revised estimates of ocean surface drag in strong winds. *Geophys. Res. Lett.*, **47**, e2020GL087647, https://doi.org/10.1029/2020GL087647.

DeCosmo, J., K. Katsaros, S. Smith, R. Anderson, W. Oost, K. Bumke, and H. Chadwick, 1996: Air-sea exchange of water vapor and sensible heat: The Humidity Exchange over the Sea (HEXOS) results. *J. Geophys. Res.*, **101**, 12 001–12 016, https://doi.org/10.1029/95JC03796.

De Leeuw, G., E. L Andreas, M. D. Anguelova, C. Fairall, E. R. Lewis, C. O'Dowd, M. Schulz, and S. E. Schwartz, 2011: Production flux of sea spray aerosol. *Rev. Geophys.*, **49**, RG2001, https://doi.org/10.1029/2010RG000349.

Donelan, M. A., B. K. Haus, N. Reul, W. J. Plant, M. Stiassnie, H. C. Graber, O. B. Brown, and E. S. Saltzman, 2004: On the limiting aerodynamic roughness of the ocean in very strong winds. *Geophys. Res. Lett.*, **31**, L18306, https://doi.org/10.1029/2004GL019460.

Drennan, W. M., J. A. Zhang, J. R. French, C. McCormick, and P. G. Black, 2007: Turbulent fluxes in the hurricane boundary layer. Part II: Latent heat flux. *J. Atmos. Sci.*, **64**, 1103–1115, https://doi.org/10.1175/JAS3889.1.

Edson, J. B., 1989: Lagrangian model simulation of the turbulent transport of evaporating jet droplets. Ph.D. thesis, The Pennsylvania State University, 154 pp.

——, and C. Fairall, 1994: Spray droplet modeling: 1. Lagrangian model simulation of the turbulent transport of evaporating droplets. *J. Geophys. Res.*, **99**, 25 295–25 311, https://doi.org/10.1029/94JC01883.

——, ——, S. E. Larsen, and P. Mestayer, 1988: A random walk simulation of the turbulent transport of evaporating jet drops in the air-sea simulation tunnel during HEXIST. *Proc. 7th Conf. on Ocean-Atmosphere Interaction*, Anaheim, CA, Amer. Meteor. Soc., 9–13.

——, S. Anquetin, P. Mestayer, and J. Sini, 1996: Spray droplet modeling: 2. An interactive Eulerian-Lagrangian model of evaporating spray droplets. *J. Geophys. Res. Oceans*, **101**, 1279–1293, https://doi.org/10.1029/95JC03280.

Emanuel, K., 1986: An air-sea interaction theory for tropical cyclones. Part I: Steady-state maintenance. *J. Atmos. Sci.*, **43**, 585–605, https://doi.org/10.1175/1520-0469(1986)043<0585:AASITF>2.0.CO;2.

——, 1995: Sensitivity of tropical cyclones to surface exchange coefficients and a revised steady-state model incorporating eye dynamics. *J. Atmos. Sci.*, **52**, 3969–3976, https://doi.org/10.1175/1520-0469(1995)052<3969:SOTCTS>2.0.CO;2.

——, 2003: A similarity hypothesis for air–sea exchange at extreme wind speeds. *J. Atmos. Sci.*, **60**, 1420–1428, https://doi.org/10.1175/1520-0469(2003)060<1420:ASHFAE>2.0.CO;2.

Fairall, C. W., 1990: Modelling the fate and influence of marine spray. *Modelling the Fate and Influence of Marine Spray: Proceedings*, P. Mestayer, E. C. Monahan, and P. A. Beetham, Eds., Whitecap Rep. 7, Marine Sciences Institute, University of Connecticut, 1–5.

——, J. Kepert, and G. Holland, 1994: The effect of sea spray on surface energy transports over the ocean. *Global Atmos. Ocean Syst.*, **2**, 121–142.

——, E. F. Bradley, D. P. Rogers, J. B. Edson, and G. S. Young, 1996: Bulk parameterization of air-sea fluxes for Tropical Ocean-Global Atmosphere Coupled-Ocean Atmosphere Response Experiment difference relative analysis. *J. Geophys. Res.*, **101**, 3747–3764, https://doi.org/10.1029/95JC03205.

——, ——, J. Hare, A. A. Grachev, and J. B. Edson, 2003: Bulk parameterization of air–sea fluxes: Updates and verification for the COARE algorithm. *J. Climate*, **16**, 571–591, https://doi.org/10.1175/1520-0442(2003)016<0571:BPOASF>2.0.CO;2.

——, M. L. Banner, W. L. Peirson, W. Asher, and R. P. Morison, 2009: Investigation of the physical scaling of sea spray spume droplet production. *J. Geophys. Res.*, **114**, C10001, https://doi.org/10.1029/2008JC004918.

French, J. R., W. M. Drennan, J. A. Zhang, and P. G. Black, 2007: Turbulent fluxes in the hurricane boundary layer. Part I: Momentum flux. *J. Atmos. Sci.*, **64**, 1089–1102, https://doi.org/10.1175/JAS3887.1.

Garg, N., E. Y. K. Ng, and S. Narasimalu, 2018: The effects of sea spray and atmosphere–wave coupling on air–sea exchange during a tropical cyclone. *Atmos. Chem. Phys.*, **18**, 6001–6021, https://doi.org/10.5194/acp-18-6001-2018.

Golbraikh, E., and Y. M. Shtemler, 2016: Foam input into the drag coefficient in hurricane conditions. *Dyn. Atmos. Oceans*, **73**, 1–9, https://doi.org/10.1016/j.dynatmoce.2015.10.005.

——, and ——, 2020: Momentum and heat transfer across the foam-covered air-sea interface in hurricanes. *Ocean Dyn.*, **70**, 683–692, https://doi.org/10.1007/s10236-020-01360-w.

Green, B. W., and F. Zhang, 2013: Impacts of air–sea flux parameterizations on the intensity and structure of tropical cyclones. *Mon. Wea. Rev.*, **141**, 2308–2324, https://doi.org/10.1175/MWR-D-12-00274.1.

——, and ——, 2014: Sensitivity of tropical cyclone simulations to parametric uncertainties in air–sea fluxes and implications for parameter estimation. *Mon. Wea. Rev.*, **142**, 2290–2308, https://doi.org/10.1175/MWR-D-13-00208.1.

Haus, B. K., D. Jeong, M. A. Donelan, J. A. Zhang, and I. Savelyev, 2010: Relative rates of sea-air heat transfer and frictional drag in very high winds. *Geophys. Res. Lett.*, **37**, L07802, https://doi.org/10.1029/2009GL042206.

Hawkins, H. F., and D. T. Rubsam, 1968: Hurricane Hilda, 1964 II. Structure and budgets of the hurricane on October 1, 1964. *Mon. Wea. Rev.*, **96**, 617–636, https://doi.org/10.1175/1520-0493(1968)096<0617:HH>2.0.CO;2.

Helgans, B., and D. H. Richter, 2016: Turbulent latent and sensible heat flux in the presence of evaporative droplets. *Int. J. Multiph. Flow*, **78**, 1–11, https://doi.org/10.1016/j.ijmultiphaseflow.2015.09.010.

Holthuijsen, L. H., M. D. Powell, and J. D. Pietrzak, 2012: Wind and waves in extreme hurricanes. *J. Geophys. Res.*, **117**, C09003, https://doi.org/10.1029/2012JC007983.

Iida, N., Y. Toba, and M. Chaen, 1992: A new expression for the production rate of sea water droplets on the sea surface. *J. Oceanogr.*, **48**, 439–460, https://doi.org/10.1007/BF02234020.

Jarosz, E., D. A. Mitchell, D. W. Wang, and W. J. Teague, 2007: Bottom-up determination of air-sea momentum exchange under a major tropical cyclone. *Science*, **315**, 1707–1709, https://doi.org/10.1126/science.1136466.

Jeong, D., B. K. Haus, and M. A. Donelan, 2012: Enthalpy transfer across the air–water interface in high winds including spray. *J. Atmos. Sci.*, **69**, 2733–2748, https://doi.org/10.1175/JAS-D-11-0260.1.

Joly, A., and Coauthors, 1997: The Fronts and Atlantic Storm-Track Experiment (FASTEX): Scientific objectives and experimental design. *Bull. Amer. Meteor. Soc.*, **78**, 1917–1940, https://doi.org/10.1175/1520-0477(1997)078<1917:TFAAST>2.0.CO;2.

Katsaros, K. B., S. D. Smith, and W. A. Oost, 1987: HEXOS—Humidity Exchange over the Sea: A program for research on water-vapor and droplet fluxes from sea to air at moderate to high wind speeds. *Bull. Amer. Meteor. Soc.*, **68**, 466–476, https://doi.org/10.1175/1520-0477(1987)068<0466:HEOTSA>2.0.CO;2.

Kleinschmidt, E., 1951: Grundlagen einer Theorie der tropischen Zyklonen. *Arch. Meteor. Geophys. Bioklimatol.*, **4A**, 53–72, https://doi.org/10.1007/BF02246793.

Koga, M., and Y. Toba, 1981: Droplet distribution and dispersion processes on breaking wind waves. *Tohoku Geophys. J.*, **28**, 1–25.

Komori, S., K. Iwano, N. Takagaki, R. Onishi, R. Kurose, K. Takahashi, and N. Suzuki, 2018: Laboratory measurements of heat transfer and drag coefficients at extremely high wind speeds. *J. Phys. Oceanogr.*, **48**, 959–974, https://doi.org/10.1175/JPO-D-17-0243.1.

Kudryavtsev, V. N., 2006: On the effect of sea drops on the atmospheric boundary layer. *J. Geophys. Res.*, **111**, C07020, https://doi.org/10.1029/2005JC002970.

Lewis, E. R., R. Lewis, K. E. Karlstrom, E. R. Lewis, and S. E. Schwartz, 2004: *Sea Salt Aerosol Production: Mechanisms, Methods, Measurements, and Models*. *Geophys. Monogr.*, Vol. 152, Amer. Geophys. Union, 413 pp.

Ling, S., and T. Kao, 1976: Parameterization of the moisture and heat transfer process over the ocean under whitecap sea states. *J. Phys. Oceanogr.*, **6**, 306–315, https://doi.org/10.1175/1520-0485(1976)006<0306:POTMAH>2.0.CO;2.

Liu, B., H. Liu, L. Xie, C. Guan, and D. Zhao, 2011: A coupled atmosphere–wave–ocean modeling system: Simulation of the intensity of an idealized tropical cyclone. *Mon. Wea. Rev.*, **139**, 132–152, https://doi.org/10.1175/2010MWR3396.1.

Ma, H., A. V. Babanin, and F. Qiao, 2020: Field observations of sea spray under tropical cyclone Olwyn. *Ocean Dyn.*, **70**, 1439–1448, https://doi.org/10.1007/s10236-020-01408-x.

Ma, Y., N. E. Davidson, Y. Xiao, and J.-W. Bao, 2017: Revised parameterization of air–sea exchanges in high winds for operational numerical prediction: Impact on tropical cyclone track, intensity, and rapid intensification. *Wea. Forecasting*, **32**, 821–848, https://doi.org/10.1175/WAF-D-15-0109.1.

Makin, V. K., 2005: A note on the drag of the sea surface at hurricane winds. *Bound.-Layer Meteor.*, **115**, 169–176, https://doi.org/10.1007/s10546-004-3647-x.

Malkus, J. S., and H. Riehl, 1960: On the dynamics and energy transformations in steady-state hurricanes. *Tellus*, **12**, 1–20, https://doi.org/10.3402/tellusa.v12i1.9351.

Mehta, S., D. G. Ortiz-Suslow, A. Smith, and B. Haus, 2019: A laboratory investigation of spume generation in high winds for fresh and seawater. *J. Geophys. Res. Atmos.*, **124**, 11 297–11 312, https://doi.org/10.1029/2019JD030928.

Mestayer, P. G., and C. Lefauconnier, 1988: Spray droplet generation, transport, and evaporation in a wind wave tunnel during the humidity exchange over the sea experiments in the simulation tunnel. *J. Geophys. Res.*, **93**, 572–586, https://doi.org/10.1029/JC093iC01p00572.

——, J. B. Edson, C. W. Fairall, S. E. Larsen, and D. E. Spiel, 1989: Turbulent transport and evaporation of droplets generated at an air-water interface. *Turbulent Shear Flows*, J.-C. André et al., Eds., Springer, 129–147.

——, A. Van Eijk, G. De Leeuw, and B. Tranchant, 1996: Numerical simulation of the dynamics of sea spray over the waves. *J. Geophys. Res.*, **101**, 20 771–20 797, https://doi.org/10.1029/96JC01425.

Miller, B. I., 1962: On the momentum and energy balance of Hurricane Helene (1958). Tech. Rep. 53, US Department of Commerce, 19 pp.

Monin, A., and A. Obukhov, 1954: Basic laws of turbulent mixing in the surface layer of the atmosphere. *Tr. Geofiz. Inst., Akad. Nauk SSSR*, **24**, 163–187.

Mueller, J. A., and F. Veron, 2009a: A sea state-dependent spume generation function. *J. Phys. Oceanogr.*, **39**, 2363–2372, https://doi.org/10.1175/2009JPO4113.1.

——, and ——, 2009b: A Lagrangian stochastic model for heavy particle dispersion in the atmospheric marine boundary layer. *Bound.-Layer Meteor.*, **130**, 229–247, https://doi.org/10.1007/s10546-008-9340-8.

——, and ——, 2009c: Nonlinear formulation of the bulk surface stress over breaking waves: Feedback mechanisms from airflow separation. *Bound.-Layer Meteor.*, **130**, 117–134, https://doi.org/10.1007/s10546-008-9334-6.

——, and ——, 2010a: A Lagrangian stochastic model for sea-spray evaporation in the atmospheric marine boundary layer. *Bound.-Layer Meteor.*, **137**, 135–152, https://doi.org/10.1007/s10546-010-9520-1.

——, and ——, 2010b: Bulk formulation of the heat and water vapor fluxes at the air–sea interface, including nonmolecular contributions. *J. Atmos. Sci.*, **67**, 234–247, https://doi.org/10.1175/2009JAS3061.1.

——, and ——, 2014a: Impact of sea spray on air–sea fluxes. Part I: Results from stochastic simulations of sea spray drops over the ocean. *J. Phys. Oceanogr.*, **44**, 2817–2834, https://doi.org/10.1175/JPO-D-13-0245.1.

——, and ——, 2014b: Impact of sea spray on air–sea fluxes. Part II: Feedback effects. *J. Phys. Oceanogr.*, **44**, 2835–2853, https://doi.org/10.1175/JPO-D-13-0246.1.

Nystrom, R. G., and F. Zhang, 2019: Practical uncertainties in the limited predictability of the record-breaking intensification of Hurricane Patricia (2015). *Mon. Wea. Rev.*, **147**, 3535–3556, https://doi.org/10.1175/MWR-D-18-0450.1.

——, X. Chen, F. Zhang, and C. A. Davis, 2020: Nonlinear impacts of surface exchange coefficient uncertainty on tropical cyclone intensity and air-sea interactions. *Geophys. Res. Lett.*, **47**, e2019GL085783, https://doi.org/10.1029/2019GL085783.

O'Dowd, C. D., and G. De Leeuw, 2007: Marine aerosol production: A review of the current knowledge. *Philos. Trans. Roy. Soc.*, **365A**, 1753–1774, https://doi.org/10.1098/rsta.2007.2043.

Ortiz-Suslow, D. G., B. K. Haus, S. Mehta, and N. J. Laxague, 2016: Sea spray generation in very high winds. *J. Atmos. Sci.*, **73**, 3975–3995, https://doi.org/10.1175/JAS-D-15-0249.1.

Palmén, E., and H. Riehl, 1957: Budget of angular momentum and energy in tropical cyclones. *J. Meteor.*, **14**, 150–159, https://doi.org/10.1175/1520-0469(1957)014<0150:BOAMAE>2.0.CO;2.

Peng, T., and D. Richter, 2017: Influence of evaporating droplets in the turbulent marine atmospheric boundary layer. *Bound.-Layer Meteor.*, **165**, 497–518, https://doi.org/10.1007/s10546-017-0285-7.

——, and ——, 2019: Sea spray and its feedback effects: Assessing bulk algorithms of air–sea heat fluxes via direct numerical simulations. *J. Phys. Oceanogr.*, **49**, 1403–1421, https://doi.org/10.1175/JPO-D-18-0193.1.

——, and ——, 2020: Influences of polydisperse sea spray size distributions on model predictions of air-sea heat fluxes.

J. Geophys. Res. Atmos., **125**, e2019JD032326, https://doi.org/10.1029/2019jd032326.

Perrie, W., W. Zhang, E. L Andreas, W. Li, J. Gyakum, and R. McTaggart-Cowan, 2005: Sea spray impacts on intensifying midlatitude cyclones. *J. Atmos. Sci.*, **62**, 1867–1883, https://doi.org/10.1175/JAS3436.1.

Persson, P., J. Hare, C. Fairall, and W. Otto, 2005: Air–sea interaction processes in warm and cold sectors of extratropical cyclonic storms observed during FASTEX. *Quart. J. Roy. Meteor. Soc.*, **131**, 877–912, https://doi.org/10.1256/jq.03.181.

Powell, M. D., P. J. Vickery, and T. A. Reinhold, 2003: Reduced drag coefficient for high wind speeds in tropical cyclones. *Nature*, **422**, 279–283, https://doi.org/10.1038/nature01481.

Pruppacher, H. R., and J. D. Klett, 1978: *Microphysics of Clouds and Precipitation*. Springer, 9–55.

Richter, D. H., and D. P. Stern, 2014: Evidence of spray-mediated air-sea enthalpy flux within tropical cyclones. *Geophys. Res. Lett.*, **41**, 2997–3003, https://doi.org/10.1002/2014GL059746.

——, R. Bohac, and D. P. Stern, 2016: An assessment of the flux profile method for determining air–sea momentum and enthalpy fluxes from dropsonde data in tropical cyclones. *J. Atmos. Sci.*, **73**, 2665–2682, https://doi.org/10.1175/JAS-D-15-0331.1.

——, A. E. Dempsey, and P. P. Sullivan, 2019: Turbulent transport of spray droplets in the vicinity of moving surface waves. *J. Phys. Oceanogr.*, **49**, 1789–1807, https://doi.org/10.1175/JPO-D-19-0003.1.

Riehl, H., 1950: A model of hurricane formation. *J. Appl. Phys.*, **21**, 917–925, https://doi.org/10.1063/1.1699784.

——, 1954: *Tropical Meteorology*. McGraw-Hill, 392 pp.

Rouault, M. P., P. G. Mestayer, and R. Schiestel, 1991: A model of evaporating spray droplet dispersion. *J. Geophys. Res.*, **96**, 7181–7200, https://doi.org/10.1029/90JC02569.

Shpund, J., M. Pinsky, and A. Khain, 2011: Microphysical structure of the marine boundary layer under strong wind and spray formation as seen from simulations using a 2D explicit microphysical model. Part I: The impact of large eddies. *J. Atmos. Sci.*, **68**, 2366–2384, https://doi.org/10.1175/2011JAS3652.1.

——, J. Zhange, M. Pinsky, and A. Khain, 2012: Microphysical structure of the marine boundary layer under strong wind and spray formation as seen from simulations using a 2D explicit microphysical model. Part II: The role of sea spray. *J. Atmos. Sci.*, **69**, 3501–3514, https://doi.org/10.1175/JAS-D-11-0281.1.

——, J. Zhang, M. Pinsky, and A. Khain, 2014: Microphysical structure of the marine boundary layer under strong wind and sea spray formation as seen from a 2D explicit microphysical model. Part III: Parameterization of height-dependent droplet size distribution. *J. Atmos. Sci.*, **71**, 1914–1934, https://doi.org/10.1175/JAS-D-12-0201.1.

Skamarock, W. C., and Coauthors, 2008: A description of the Advanced Research WRF version 3. NCAR Tech. Note NCAR/TN-475+STR, 113 pp., https://doi.org/10.5065/D68S4MVH.

Smith, M., P. Park, and I. Consterdine, 1993: Marine aerosol concentrations and estimated fluxes over the sea. *Quart. J. Roy. Meteor. Soc.*, **119**, 809–824, https://doi.org/10.1002/qj.49711951211.

Soloviev, A. V., R. Lukas, M. A. Donelan, B. K. Haus, and I. Ginis, 2014: The air-sea interface and surface stress under tropical cyclones. *Sci. Rep.*, **4**, 5306, https://doi.org/10.1038/srep05306.

——, ——, ——, ——, and ——, 2017: Is the state of the air-sea interface a factor in rapid intensification and rapid decline of tropical cyclones? *J. Geophys. Res. Oceans*, **122**, 10 174–10 183, https://doi.org/10.1002/2017JC013435.

Toba, Y., and M. Koga, 1986: A parameter describing overall conditions of wave breaking, whitecapping, sea-spray production and wind stress. *Oceanic Whitecaps*, E. C. Monahan and G. M. Niocaill, Eds., Springer, 37–47.

——, S. Komori, Y. Suzuki, and D. Zhao, 2006: Similarity and dissimilarity in air-sea momentum and CO_2 transfers: The nondimensional transfer coefficients in light of windsea Reynolds number. *Atmosphere-Ocean Interactions*, Vol. 2, W. Perrie, Ed., WIT Press, 53–82.

Toffoli, A., A. Babanin, M. Donelan, B. Haus, and D. Jeong, 2011: Estimating sea spray volume with a laser altimeter. *J. Atmos. Oceanic Technol.*, **28**, 1177–1183, https://doi.org/10.1175/2011JTECHO827.1.

Torn, R. D., 2016: Evaluation of atmosphere and ocean initial condition uncertainty and stochastic exchange coefficients on ensemble tropical cyclone intensity forecasts. *Mon. Wea. Rev.*, **144**, 3487–3506, https://doi.org/10.1175/MWR-D-16-0108.1.

Troitskaya, Y. I., D. Sergeev, A. Kandaurov, G. Baidakov, M. Vdovin, and V. Kazakov, 2012: Laboratory and theoretical modeling of air-sea momentum transfer under severe wind conditions. *J. Geophys. Res.*, **117**, C00J21, https://doi.org/10.1029/2011JC007778.

Troitskaya, Y., D. A. Sergeev, O. Druzhinin, A. A. Kandaurov, O. S. Ermakova, E. V. Ezhova, I. Esau, and S. Zilitinkevich, 2014: Atmospheric boundary layer over steep surface waves. *Ocean Dyn.*, **64**, 1153–1161, https://doi.org/10.1007/s10236-014-0743-4.

——, A. Kandaurov, O. Ermakova, D. Kozlov, D. Sergeev, and S. Zilitinkevich, 2017: Bag-breakup fragmentation as the dominant mechanism of sea-spray production in high winds. *Sci. Rep.*, **7**, 1614, https://doi.org/10.1038/s41598-017-01673-9.

——, ——, ——, ——, ——, and ——, 2018a: The ''bag breakup'' spume droplet generation mechanism at high winds. Part I: Spray generation function. *J. Phys. Oceanogr.*, **48**, 2167–2188, https://doi.org/10.1175/JPO-D-17-0104.1.

——, O. Druzhinin, D. Kozlov, and S. Zilitinkevich, 2018b: The ''bag breakup'' spume droplet generation mechanism at high winds. Part II: Contribution to momentum and enthalpy transfer. *J. Phys. Oceanogr.*, **48**, 2189–2207, https://doi.org/10.1175/JPO-D-17-0105.1.

——, D. Sergeev, A. Kandaurov, M. Vdovin, and S. Zilitinkevich, 2019: The effect of foam on waves and the aerodynamic roughness of the water surface at high winds. *J. Phys. Oceanogr.*, **49**, 959–981, https://doi.org/10.1175/JPO-D-18-0168.1.

——, ——, M. Vdovin, A. Kandaurov, O. Ermakova, and N. Takagaki, 2020: A laboratory study of the effect of surface waves on heat and momentum transfer at high wind speeds. *J. Geophys. Res. Oceans*, **125**, e2020JC016276, https://doi.org/10.1029/2020JC016276.

Van Eijk, A. M., B. S. Tranchant, and P. G. Mestayer, 2001: SeaCluse: Numerical simulation of evaporating sea spray droplets. *J. Geophys. Res.*, **106**, 2573–2588, https://doi.org/10.1029/2000JC000377.

Vanderplow, B., A. V. Soloviev, C. W. Dean, B. K. Haus, R. Lukas, M. Sami, and I. Ginis, 2020: Potential effect of bio-surfactants on sea spray generation in tropical cyclone conditions. *Sci. Rep.*, **10**, 19057, https://doi.org/10.1038/s41598-020-76226-8.

Veron, F., 2015: Ocean spray. *Annu. Rev. Fluid Mech.*, **47**, 507–538, https://doi.org/10.1146/annurev-fluid-010814-014651.

——, C. Hopkins, E. L. Harrison, and J. A. Mueller, 2012: Sea spray spume droplet production in high wind speeds. *Geophys. Res. Lett.*, **39**, L16602, https://doi.org/10.1029/2012GL052603.

Vickery, P. J., D. Wadhera, M. D. Powell, and Y. Chen, 2009: A hurricane boundary layer and wind field model for use in engineering applications. *J. Appl. Meteor. Climatol.*, **48**, 381–405, https://doi.org/10.1175/2008JAMC1841.1.

Wada, A., S. Kanada, and H. Yamada, 2018: Effect of air-sea environmental conditions and interfacial processes on extremely intense Typhoon Haiyan (2013). *J. Geophys. Res. Atmos.*, **123**, 10 379–10 405, https://doi.org/10.1029/2017JD028139.

Wu, J., J. J. Murray, and R. J. Lai, 1984: Production and distributions of sea spray. *J. Geophys. Res.*, **89**, 8163–8169, https://doi.org/10.1029/JC089iC05p08163.

Zhang, J. A., P. G. Black, J. R. French, and W. M. Drennan, 2008: First direct measurements of enthalpy flux in the hurricane boundary layer: The CBLAST results. *Geophys. Res. Lett.*, **35**, L14813, https://doi.org/10.1029/2008GL034374.

Zhao, D., and Y. Toba, 2001: Dependence of whitecap coverage on wind and wind-wave properties. *J. Oceanogr.*, **57**, 603–616, https://doi.org/10.1023/A:1021215904955.

——, ——, Y. Suzuki, and S. Komori, 2003: Effect of wind waves on air–sea gas exchange: Proposal of an overall CO_2 transfer velocity formula as a function of breaking-wave parameter. *Tellus*, **55B**, 478–487, https://doi.org/10.3402/tellusb.v55i2.16747.

——, ——, K. I. Sugioka, and S. Komori, 2006: New sea spray generation function for spume droplets. *J. Geophys. Res.*, **111**, C02007, https://doi.org/10.1029/2005JC002960.

Zou, Z., D. Zhao, J. Tian, B. Liu, and J. Huang, 2018: Drag coefficients derived from ocean current and temperature profiles at high wind speeds. *Tellus*, **70A**, 1–13, https://doi.org/10.1080/16000870.2018.1463805.